

Article

Experimental and Theoretical Investigation of Viscoelastic Damper by Applying Fractional Derivative Method and Internal Variable Theory

Yeshou Xu ^{1,*}, Qi He ¹, Ying-Qing Guo ^{2,3}, Xing-Huai Huang ¹, Yao-Rong Dong ⁴, Zhong-Wei Hu ¹ and Jinkoo Kim ⁵

¹ China-Pakistan Belt and Road Joint Laboratory on Smart Disaster Prevention of Major Infrastructures, Southeast University, Nanjing 211189, China

² Mechanical and Electronic Engineering School, Nanjing Forestry University, Nanjing 210037, China

³ Nanjing Dongrui Damping Control Technology Co., Ltd., Nanjing 210033, China

⁴ School of Civil Engineering, Xi'an University of Architecture and Technology, Xi'an 710055, China

⁵ Department of Civil and Architectural Engineering, Sungkyunkwan University, Suwon 030603, Republic of Korea

* Correspondence: xuyeshou@163.com

Abstract: Viscoelastic dampers are conventional passive vibration control devices with excellent energy dissipation performance. The fractional derivative has a simple form and high accuracy in the modelling of viscoelastic materials/dampers. The internal variables reflect the internal state evolution of materials, and are often used to analyze the deformation and thermal process of materials. In the present work, the mechanical properties of a plate-shear-type viscoelastic damper at room temperature are tested under sinusoidal displacement excitations. The impacts of frequency and displacement amplitude on the dynamic properties of the viscoelastic damper in a wide frequency domain (0.1–25 Hz) are investigated. The higher-order fractional derivative model and the temperature–frequency equivalent principle are employed to characterize the frequency and temperature influence, and the internal variable theory considering the internal/microscale structure evolutions is introduced to capture the displacement affection. The higher-order fractional derivative model modified with the internal variable theory and temperature–frequency equivalent principle (ITHF) is accurate enough in describing the dynamic behaviors of viscoelastic dampers with varying frequencies and displacement amplitudes.

Keywords: viscoelastic damper; mechanical properties test; higher-order fractional derivative model; temperature–frequency equivalent principle; internal variable theory



Citation: Xu, Y.; He, Q.; Guo, Y.-Q.; Huang, X.-H.; Dong, Y.-R.; Hu, Z.-W.; Kim, J. Experimental and Theoretical Investigation of Viscoelastic Damper by Applying Fractional Derivative Method and Internal Variable Theory. *Buildings* **2023**, *13*, 239. <https://doi.org/10.3390/buildings13010239>

Academic Editor: Marco Di Ludovico

Received: 15 December 2022

Revised: 9 January 2023

Accepted: 12 January 2023

Published: 14 January 2023



Copyright: © 2023 by the authors. Licensee MDPI, Basel, Switzerland. This article is an open access article distributed under the terms and conditions of the Creative Commons Attribution (CC BY) license (<https://creativecommons.org/licenses/by/4.0/>).

1. Introduction

Viscoelastic dampers are perfect energy dissipation devices and have been widely used in seismic/wind vibration control, micro vibration suppression, and platform vibration isolation, etc. [1–4]. The damping performance and energy dissipation capacity of viscoelastic dampers mainly depend on the mechanical properties of viscoelastic materials [5]. Scholars have accomplished a lot of achievements in the research of viscoelastic materials and dampers [6–9].

In 1992, Zhang et al. [10] proposed a sequential design procedure for optimal placement of viscoelastic dampers in structures, and experimentally verified it with a five-story steel model structure. Aprile et al. [11] studied the influence of loading frequency and displacement amplitude on the dynamic modulus of viscoelastic dampers. Tsai et al. [12] investigated the temperature impacts on the seismic control effect of viscoelastically damped building structures. Viscoelastic dampers can effectively reduce seismic responses of structures, and the damping effect decreases with the increment in temperature. Cazenove

et al. [13] conducted numerical and theoretical observations on the self-heating effect of viscoelastic dampers. The results show that the self-heating phenomenon of viscoelastic dampers is very important and should not be neglected in vibration control analysis and structural design. Xu et al. studied the damping properties of viscoelastic dampers with different viscoelastic materials [5,14], and utilized the shaking table test to study the seismic response of structure models retrofitted with viscoelastic dampers [15–18]. Sato et al. [19] proposed an evaluation method for the practical application of viscoelastic dampers in wind vibration control by using equivalent sinusoidal waveforms of long-duration random excitations in along- and across-wind directions. Xu et al. [20] proposed a micro-vibration isolation and mitigation platform with four viscoelastic damper components to reduce disturbance generated by flywheels onboard spacecraft. He et al. [21] designed a new type of viscoelastic damper to control the translational vibration and the rotational vibration of offshore platforms simultaneously, and shaking table tests were conducted to verify the capability of dampers in mitigating the multi-dimensional seismic responses of platforms.

The dynamic characteristics and energy dissipation performance of viscoelastic dampers show a significantly nonlinear variation trend with varying temperatures, frequencies, and loading displacement amplitudes. The appropriate mathematical model is conducive to more efficient characterization of mechanical properties of dampers and response analysis of viscoelastic damper-retrofitted structures. Traditional constitutive models, the Kelvin model, Maxwell model, Zener model, and fractional derivative models, etc. [22], of viscoelastic materials are mature in characterizing frequency dependence and rheological properties, but the temperature and frequency reliance of materials cannot be reflected well. Tsai [23] established a finite element model for viscoelastic dampers by using a fractional derivative operator and empirical formula to consider the dependence of temperature, frequency, and displacement amplitude at the same time. However, it is rarely utilized by researchers due to its complex form. Payne et al. [24] assumed that the displacement dependence of the material was mainly due to the influence of the micro filler network system, and used the Kraus model to explain the correlation characteristics between dynamic properties of the damper and displacement amplitudes. Liang et al. [25] built a constitutive model of viscoelastic materials based on a complex combination of multiple relaxation viscoelastic and viscoplastic models, which can predict the remarkable temperature- and rate-dependent deformation behaviors of materials well. Bagley et al. [26] and Lewandowski [27] investigated the mechanical behavior of viscoelastic materials and conducted a structural seismic analysis of damping structures based on fractional derivative theory, which has a more concise form and higher accuracy than integral derivative models. Xu et al. [28,29] formulated the temperature–frequency equivalent principle based on the W-L-F equation, and theoretically translated the effects of temperature into frequency impacts. Conti et al. [30] proposed a new mathematical model to describe the aging effects of viscoelastic materials. The convolution kernel of the integro-differential equation for describing the viscoelasticity was redefined as a function of time. Wang et al. [31] theoretically studied the macro properties of viscoelastic materials with the assumption that the multi-layer molecular networks interpenetrated together with different chain lengths. Lu et al. [32] investigated the constitutive relation of viscoelastic materials considering the friction effect of single molecular chains from surrounding environments at the microscale.

Most of the aforementioned research considers the constitutive relationship and mechanical properties of viscoelastic materials from the macroperspective, and there are few examples of literature from the microperspective. In traditional thermodynamic theories, the state of materials at an arbitrary moment determined by the macro variables, deformation, temperature, etc., and the internal variables, which could be one or a set of state variables, such as the damage accumulation, nonelastic deformation, phase transformation, free volume variation, and changes in material particle size, etc. [33,34]. The internal variables reflect the evolution process of the internal structure state of materials, and affect the macro mechanical properties and damping performance of viscoelastic materials significantly. The purpose of the present research is to study the dynamic performance of

viscoelastic dampers with different frequencies and displacements at room temperature, and theoretically propose new mathematical models with fractional derivative and internal variable theory. The mechanical properties of a plate-shear type-viscoelastic damper at room temperature are tested under sinusoidal displacement excitations. The impacts of frequency and displacement amplitude on the dynamic properties of a viscoelastic damper in a wide frequency domain (0.1–25 Hz) are investigated. The higher-order fractional derivative model and the temperature–frequency equivalent principle are employed to predict the dynamic property variation of the damper with frequency and temperature changes, and the internal variable theory considering the internal/microscale structure evolutions is introduced to capture the displacement affection. The higher-order fractional derivative model modified with the internal variable theory and temperature–frequency equivalent principle (ITHF) is accurate enough and more appropriate than the higher-order fractional derivative model modified with the Kraus model and temperature–frequency equivalent principle (KTHF) in describing the dynamic performance of viscoelastic dampers with varying temperatures, frequencies, and displacement amplitudes.

2. Performance Test

To study the dynamic properties and vibration reduction efficiency of the viscoelastic damper with a wide frequency range (0.1~25 Hz), the hydraulic servo fatigue tests were conducted under external excitations with different loading frequencies and displacement amplitudes. The results show that the viscoelastic damper has great efficiency in energy dissipation. The properties parameters storage modulus, loss modulus, loss factor, energy dissipation, equivalent stiffness, and equivalent damping are importantly affected by the excitation frequency, and the impact of displacement amplitude on properties parameters of the viscoelastic damper is relatively slight.

2.1. Test Situation

The viscoelastic damper is fabricated based on the nitrile rubber matrix, and composed of three steel plates and two viscoelastic layers in parallel, as shown in Figure 1b. The dimensions of the viscoelastic layers are 60 mm × 50 mm × 10 mm. During the performance tests, the viscoelastic layers undergo simple shear deformation along the length direction of the damper and the external mechanical energy can be dissipated through the shear deformation. The dynamic performance tests of the damper are conducted with a 100 kN hydraulic servo fatigue test machine manufactured by w+b Company, Switzerland, as seen in Figure 1a. The viscoelastic damper is fixed tightly on the machine by steel joints and bolts (see Figure 1b). A temperature controlling box is utilized to adjust the environmental temperature to 18 °C, and the viscoelastic damper is put inside an incubator to make the temperature stable. The external displacement excitation $u_d = u_0 \sin(\omega t)$ is applied to the viscoelastic damper, where u_d is the displacement of the damper and u_0 denotes the displacement amplitude. ω is angular frequency and $\omega = 2\pi f$, where f denotes the loading frequency and t is time. All the test conditions of the viscoelastic damper are given in Table 1, and the force and displacement at each test condition are recorded by the data record system.

Table 1. Conditions of the dynamic performance tests.

Frequencies f (Hz)	Amplitudes d (mm)	Temperature T (°C)	Cycle Number
0.1, 0.2, 0.3, 0.5, 1.0, 1.5, 2.0, 3.0, 4.0, 5.0, 7.0, 10.0, 15.0, 20.0, 25.0	0.5, 1.0, 1.5, 2.5	18	5

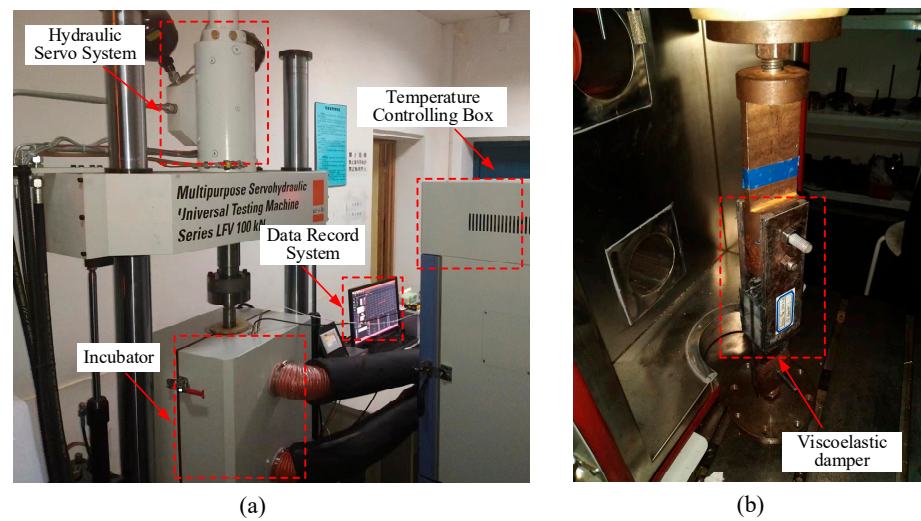


Figure 1. Dynamic properties tests of the viscoelastic damper. (a) Schematic diagram of the dynamic test. (b) Viscoelastic damper inside the incubator.

2.2. Results Analysis

To better analyze the mechanical properties and dynamic damping characteristics of the viscoelastic damper, the force–displacement hysteresis curves of the damper with changing external excitation frequencies and loading displacement amplitudes are shown in Figures 2 and 3, respectively.

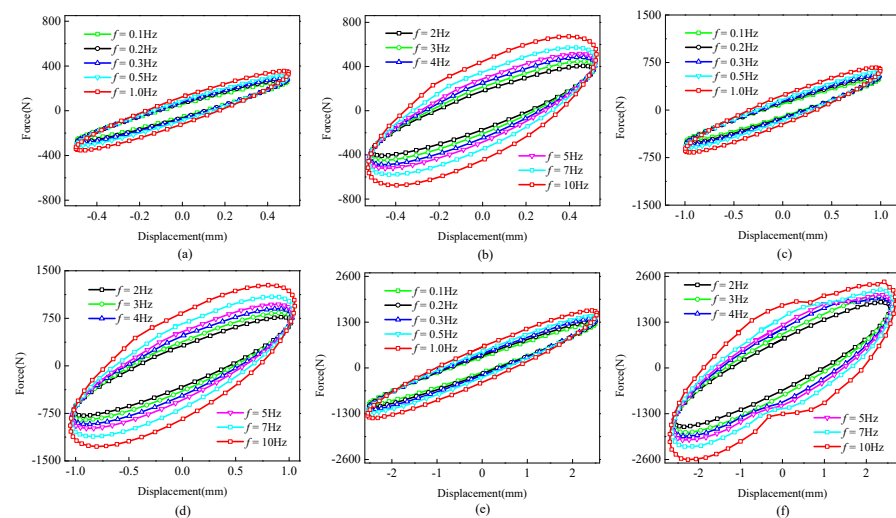


Figure 2. Hysteretic curves of the viscoelastic damper with changing frequencies. (a) $d = 0.5$ mm, $f = 0.1\sim 1$ Hz. (b) $d = 0.5$ mm, $f = 2\sim 10$ Hz. (c) $d = 1$ mm, $f = 0.1\sim 1$ Hz. (d) $d = 1$ mm, $f = 2\sim 10$ Hz. (e) $d = 2.5$ mm, $f = 0.1\sim 1$ Hz. (f) $d = 2.5$ mm, $f = 2\sim 10$ Hz.

The force–displacement curves of the viscoelastic damper with different loading frequencies are presented in Figure 2. It reveals that the viscoelastic damper has great energy dissipation properties, especially at high frequencies. The maximum damping force, major axis slope, smoothness, and plumpness of the hysteresis curve increase remarkably with increasing frequencies. Taking the maximum damping forces and areas at 0.1 Hz and 10 Hz as an example, the maximum damping forces and areas at frequency 10 Hz are almost twice of those at frequency 0.1 Hz.

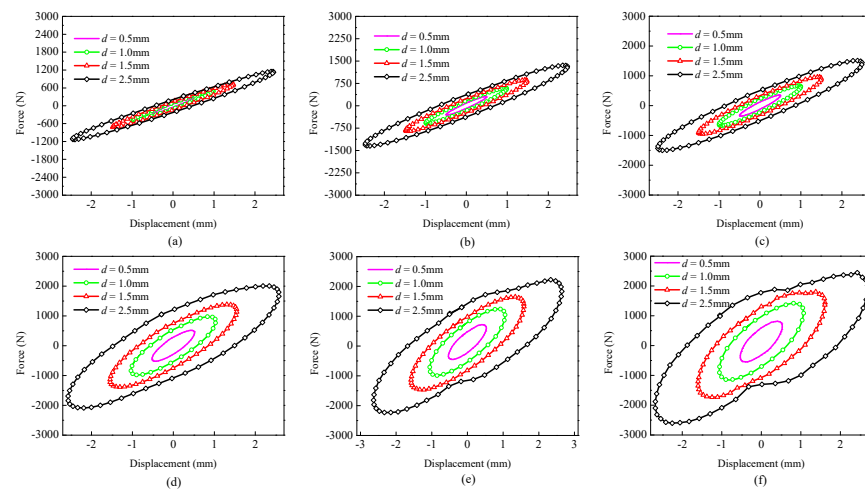


Figure 3. Hysteretic curves of the viscoelastic damper with changing displacement amplitudes. (a) $f = 0.1$ Hz. (b) $f = 0.5$ Hz. (c) $f = 1$ Hz. (d) $f = 5$ Hz. (e) $f = 7$ Hz. (f) $f = 10$ Hz.

The force–displacement curves of the viscoelastic damper with different displacement amplitudes are given in Figure 3. The damping performance of the viscoelastic damper are significantly influenced by the displacement amplitudes. The maximum damping force, smoothness, and plumpness of the force–displacement curves are increased rapidly with increasing displacement amplitudes. However, the impacts of the displacement amplitudes on the major axis slopes of the force–displacement curves are not obvious, as the equivalent stiffness changes slightly when the displacement amplitude varies from 0.5 mm to 2.5 mm.

To further analyze the mechanical properties and dynamic damping performance of the viscoelastic damper, the characteristic parameters of the viscoelastic damper storage modulus, loss modulus, loss factor, energy dissipation, equivalent stiffness, and equivalent damping at each test condition are calculated based on the force–displacement curves. According to the classical theories of viscoelastic dampers [35,36], the hysteresis curve of the viscoelastic damper can be considered as a standard ellipse as seen in Figure 4. The analytic equation of the ellipse has the form

$$\left(\frac{F_d - K_e u_d}{\eta K_e u_0}\right)^2 + \left(\frac{u_d}{u_0}\right)^2 = 1 \quad (1)$$

where u_d is the displacement and has been given as $u_d = u_0 \sin(\omega t)$ in the dynamic fatigue tests. F_d is the corresponding damping force of the viscoelastic damper at u_d . u_0 represents the displacement amplitude of the damper, and F_1 is the corresponding damping force at u_0 . K_e means the equivalent stiffness, and $K_e = F_1/u_0$. F_2 denotes the damping force when $u_d = 0$ and $\eta = F_2/F_1$. F means the biggest damping force at each hysteresis curve.

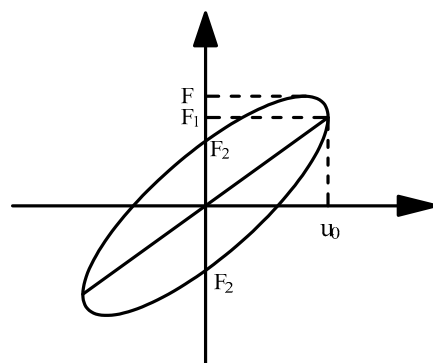


Figure 4. Force–displacement hysteresis curve.

The experimental results of the storage modulus, loss modulus, loss factor, energy dissipation, equivalent stiffness, and equivalent damping can be obtained with following equations:

$$G_1 = \frac{F_1 h_v}{n_v A_v u_0} \quad (2)$$

$$G_2 = \frac{F_2 h_v}{n_v A_v u_0} \quad (3)$$

$$\eta = \frac{F_2}{F_1} \quad (4)$$

$$E_d = \pi F_2 u_0 \quad (5)$$

$$K_e = \frac{F_1}{u_0} \quad (6)$$

$$C_e = \frac{F_2}{\omega u_0} \quad (7)$$

where G_1 denotes the storage modulus, h_v denotes the thickness of the viscoelastic layers, n_v represents the number of viscoelastic layers, and A_v means the shear area of the viscoelastic layers. For the viscoelastic damper utilized in present work, $h_v = 10$ mm, $n_v = 2$, and $A_v = 60$ mm \times 50 mm = 3000 mm². G_2 means the loss modulus and η is the loss factor. E_d is the energy dissipation at each hysteresis curve, which is calculated as the area of the ellipse. K_e is the equivalent stiffness and C_e is the equivalent damping.

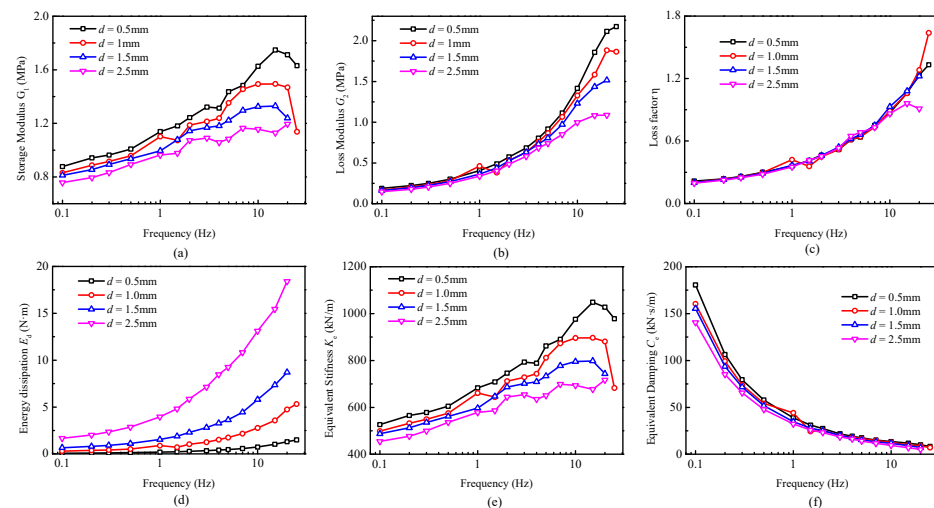
The characteristic parameters of the viscoelastic damper G_1 , G_2 , η , E_d , K_e , and C_e with changing frequencies and different amplitudes have been obtained in Tables 2 and 3, and vividly pictured in Figures 5 and 6.

Table 2. Properties parameters G_1 , G_2 , and η of the viscoelastic damper under different conditions.

Frequency f (Hz)	Displacement Amplitude d (mm)	Storage Modulus G_1 (MPa)	Loss Modulus G_2 (MPa)	Loss Factor η
0.1	0.5	0.8774	0.1891	0.2155
	1.0	0.8309	0.168	0.2022
	1.5	0.8123	0.1627	0.2002
	2.5	0.758	0.1472	0.1941
0.5	0.5	1.0082	0.3025	0.3
	1.0	0.9582	0.2836	0.296
	1.5	0.936	0.2711	0.2896
	2.5	0.8934	0.2501	0.28
1.0	0.5	1.1385	0.4071	0.3576
	1.0	1.1018	0.4627	0.42
	1.5	0.9952	0.3648	0.3666
	2.5	0.9638	0.3379	0.3506
5.0	0.5	1.4372	0.9166	0.6378
	1.0	1.3529	0.8668	0.6407
	1.5	1.2226	0.8076	0.6605
	2.5	1.0845	0.741	0.6833
10.0	0.5	1.6264	1.4151	0.8701
	1.0	1.4936	1.328	0.8891
	1.5	1.3255	1.2319	0.9294
	2.5	1.1564	0.9978	0.8628
20.0	0.5	1.7128	2.1143	1.2344
	1.0	1.4687	1.8828	1.2819
	1.5	1.2394	1.5164	1.2235
	2.5	1.1948	1.0873	0.91

Table 3. Properties parameters E_d , K_e , and C_e of the viscoelastic damper under different conditions.

Frequency f (Hz)	Displacement Amplitude d (mm)	Energy Dissipation E_d (N·m)	Equivalent Stiffness K_e (KN/m)	Equivalent Damping C_e (KN·s/m)
0.1	0.5	0.0859	526.4681	180.5752
	1.0	0.3053	498.5189	160.4234
	1.5	0.664	487.4013	155.3158
	2.5	1.6705	454.776	140.5169
0.5	0.5	0.1385	604.9157	57.7726
	1.0	0.5195	574.9053	54.1656
	1.5	1.1186	561.5877	51.7731
	2.5	2.861	536.03	47.7705
1.0	0.5	0.1906	683.0747	38.8732
	1.0	0.8881	661.0809	44.1857
	1.5	1.5401	597.1266	34.8371
	2.5	3.9516	578.3022	32.2703
5.0	0.5	0.4665	862.3496	17.5064
	1.0	1.7457	811.7594	16.5545
	1.5	3.6414	733.5588	15.4236
	2.5	9.2452	650.7179	14.1523
10.0	0.5	0.7364	975.8111	13.5127
	1.0	2.7693	896.144	12.681
	1.5	5.7994	795.3137	11.7641
	2.5	13.1152	693.8486	9.5278
20.0	0.5	1.3034	1027.6901	10.0951
	1.0	4.7438	881.2364	8.9897
	1.5	8.7057	743.6433	7.2403
	2.5	18.4049	716.8831	5.1913

**Figure 5.** Dynamic properties parameters with varying frequencies. (a) Storage modulus. (b) Loss modulus. (c) Loss factor. (d) Energy dissipation. (e) Equivalent stiffness. (f) Equivalent damping.

The variations of the characteristic parameters G_1 , G_2 , η , E_d , K_e , and C_e with increasing frequencies are shown in Figure 5. It is shown that all the dynamic parameters increase rapidly when the loading frequency increases except the equivalent damping C_e , which is reduced rapidly with frequency increment. The changing rates of the properties parameters at low frequencies (0.1~1 Hz) are much larger than those at high frequencies (1~25 Hz). Taking the test conditions with $d = 0.5$ mm as an example, the characteristic parameters' changing rates with increasing frequencies are given in Table 4. These phenomena can

be explained together with the micro structures of viscoelastic materials. The macro mechanical properties and energy dissipation performance are closely related to the micro molecular chain structures. When the frequency initially increases, the excitation time of external loading is gradually shortened, becoming closer to the molecular chain relaxation time. Therefore, the dynamic modulus and stiffness increase with increasing frequencies in 0.1~1 Hz. The excitation time of external loading is further shortened, becoming far less than the relaxation time of the molecular chains when the frequency further increases in the range of 1~25 Hz. The molecular chains cannot keep up with the movement of external excitations, and the increasing rates of dynamic modulus and stiffness are gradually decreased.

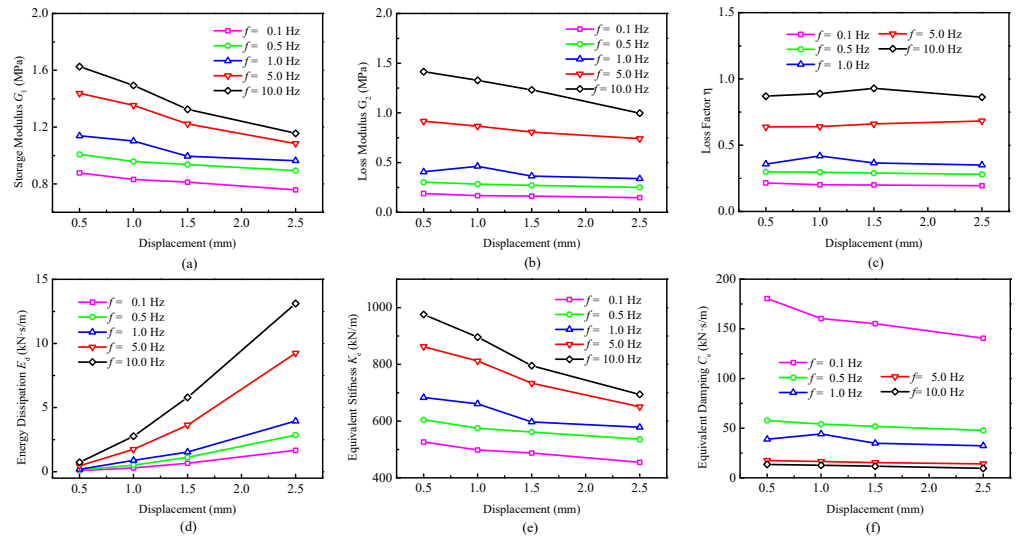


Figure 6. Dynamic properties parameters with varying displacement amplitudes. (a) Storage modulus. (b) Loss modulus. (c) Loss factor. (d) Energy dissipation. (e) Equivalent stiffness. (f) Equivalent damping.

Table 4. Parameters’ changing rate with different frequencies when $d = 0.5$ mm.

Frequency f (Hz)	0.1~0.5	0.5~1	1~5	5~10	10~20
Storage modulus G_1	+14.91%	+12.92%	+26.24%	+13.16%	+5.31%
Loss modulus G_2	+59.97%	+34.58%	+125.15%	+54.39%	+49.41%
Loss factor η	+39.21%	+19.2%	+78.36%	+36.42%	+41.87%
Energy dissipation E_d	+61.23%	+37.62%	+144.75%	+57.86%	+77%
Equivalent stiffness K_e	+14.9%	+12.92%	+26.25%	+13.16%	+5.32%
Equivalent damping C_e	−68.01%	−32.71%	−54.97%	−22.81%	−25.29%

The equivalent damping C_e decreases with the increment of frequency, which can be explained by Equation (7). Furthermore, the characteristic parameters G_1 and K_e , and G_2 and E_d have the same change ratio with increasing frequencies, because there is a positive correlation between G_1 and K_e , and G_2 and E_d , as formulated in Equations (2)–(6). In conclusion, the dynamic performance of the viscoelastic damper is significantly affected by the excitation frequency.

Figure 6 shows the dynamic parameters’ variation when displacement amplitude changes from 0.5 mm to 2.5 mm. The dynamic properties and damping parameters decrease slightly with displacement amplitude increment. This trend is more obvious at high frequencies (5 Hz and 10 Hz). The energy dissipation increases notably with the increment of excitation amplitudes. Taking the test conditions with $f = 5$ Hz as an example, the characteristic parameters’ changing rates with varying displacement amplitudes are shown in Table 5.

Table 5. Parameters' changing rate with varying displacement amplitudes when $f = 5.0$ Hz.

Displacement d (mm)	0.5~1.0	1.0~1.5	1.5~2.5
Storage modulus G_1	−5.87%	−9.63%	−11.3%
Loss modulus G_2	−5.43%	−6.83%	−8.25%
Loss factor η	+0.45%	+3.09%	+3.45%
Energy dissipation E_d	+274.21%	+108.59%	+153.89%
Equivalent stiffness K_e	−5.87%	−9.63%	−11.29%
Equivalent damping C_e	−5.44%	−6.83%	−8.24%

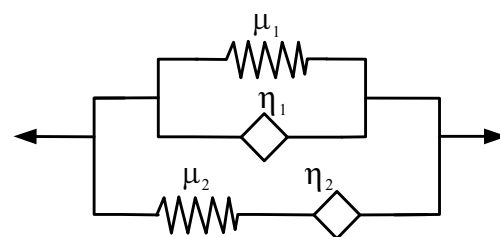
The intermolecular force, van der Waals force, between filler particles, carbon black, silicon, etc., and the micro molecular chains adsorption on filler particle surfaces significantly enhance the modulus and strength of viscoelastic materials. With the increment of displacement amplitudes, the van der Waals force between filler particles and the molecular chain adsorption will be gradually weakened, which leads to the reduction in characteristic parameters G_1 , G_2 , η , K_e , and C_e . The energy dissipation E_d clearly increases when the displacement amplitude increases, which can be explained with the positive proportional relationship shown in Equation (5). The displacement amplitudes possess slight influence on mechanical behaviors but have great significance for the damping properties of viscoelastic dampers.

3. Theoretical Modeling

From the abovementioned experimental results, it can be seen that the dynamic loading frequency and displacement amplitude are two factors that significantly affect the mechanical and energy dissipation performance of viscoelastic dampers. Accurate and reasonable mathematical models are essential to describe the dynamic behaviors of viscoelastic dampers. In this part, the higher-order fractional derivative model is modified with the internal variable theory and temperature–frequency equivalent principle to characterize the performance of viscoelastic dampers with changing frequencies, displacement amplitudes, and temperatures.

3.1. Higher-Order Fractional Derivative Model

The higher-order fractional derivative model consists of a fractional Kelvin model and a fractional Maxwell model in parallel, as shown in Figure 7, which has three fractional derivative parameters and is more accurate in describing the static creep and dynamic damping characteristics of viscoelastic materials.

**Figure 7.** The higher-order fractional derivative model.

The stress–strain expressions of the higher-order fractional derivative model has the form

$$\frac{c_2}{\eta_1} \sigma(t) + \frac{1}{\eta_1} D^\alpha \sigma(t) = D^{\alpha+\gamma} \varepsilon(t) + c_1 D^\alpha \varepsilon(t) + \frac{\mu_2}{\eta_1} D^\beta \varepsilon(t) + c_2 D^\gamma \varepsilon(t) + c_1 c_2 \varepsilon(t) \quad (8)$$

where μ_1 and μ_2 are elastic modules of the spring elements. η_1 and η_2 are viscous parameters of the fractional dashpots. $c_1 = \mu_1/\eta_1$ and $c_2 = \mu_2/\eta_2$. α , β , and γ are the α -order, β -order, and γ -order fractional derivatives, respectively.

By applying the Fourier transform to Equation (8), the complex form modulus of the higher-order fractional derivative model can be obtained as

$$G^*(\omega) = \frac{\sigma^*(\omega)}{\varepsilon^*(\omega)} = \mu_1 + \eta_1(i\omega)^\gamma + \frac{\mu_2(i\omega)^\beta}{c_2 + (i\omega)^\alpha} \quad (9)$$

The dynamic modulus can be gained by decomposing Equation (9) into two parts; the real part is the storage modulus, the imaginary part is the loss modulus, and the loss factor is the ratio of the imaginary part to the real part:

$$G_1 = \mu_1 + \eta_1\omega^\gamma \cos(\gamma\pi/2) + \frac{\mu_2c_2\omega^\beta \cos(\beta\pi/2) + \mu_2\omega^{\alpha+\beta} \cos[(\alpha - \beta)\pi/2]}{c_2^2 + 2c_2\omega^\alpha \cos(\beta\pi/2) + \omega^{2\alpha}} \quad (10)$$

$$G_2 = \eta_1\omega^\gamma \sin(\gamma\pi/2) + \frac{\mu_2c_2\omega^\beta \sin(\beta\pi/2) + \mu_2\omega^{\alpha+\beta} \sin[(\beta - \alpha)\pi/2]}{c_2^2 + 2c_2\omega^\alpha \cos(\beta\pi/2) + \omega^{2\alpha}} \quad (11)$$

$$\eta = \frac{G_2}{G_1} \quad (12)$$

3.2. Internal Variable Theory

The dynamic modulus of carbon black-filled viscoelastic materials not only has temperature and frequency dependence, but also has displacement/strain amplitude reliance. Therefore, it is of crucial significance to describe the temperature, frequency, and strain amplitude dependence of the dynamic modulus of carbon black-filled viscoelastic materials with an appropriate model. Payne et al. [24] believed that the dynamic modulus of materials decreased with increments of strain amplitudes, which was due to the destruction of the filler network structures. The energy dissipation is mainly caused by the destruction and rebuilding of the filler network structures, and the Kraus model is introduced to describe the strain amplitude influence.

Both classical irreversible thermodynamics and rational thermodynamics use internal variables to describe the thermomechanical state of materials. These internal variables are microscale state variables such as damage accumulation, phase transformation, free volume variation, grain size change, inelastic strain, stress, etc., which are impossible to be observed at the macroscale. Their changes reflect the internal state evolution of materials, and have an important impact on the deformation and thermal process of materials. The deformation history and strain amplitude have a critical influence on the viscosity of viscoelastic materials. Lion et al. [37] introduced the intrinsic time with internal variables to characterize this correlation and describe the evolution process of materials:

$$u(t) = \psi(\omega, \varepsilon_0)t \quad (13)$$

where $u(t)$ is the intrinsic time, and ε_0 denotes the excitation strain amplitude. $\psi(\omega, \varepsilon_0)$ is the reduction factor, which has the form

$$\psi(\omega, \varepsilon_0) = 1 + \frac{2}{\pi} \chi \omega^\zeta \varepsilon_0 \quad (14)$$

where χ and ζ are material parameters, and $\omega = 2\pi f$.

Based on the Riemann–Liouville-type definition, the i th order fractional derivative of stress has the form

$$D^i[\sigma(t)] = \frac{d^i}{dt^i}\sigma(t) = \frac{1}{\Gamma(1-i)} \int_0^t \frac{\dot{\sigma}(s)}{(t-s)^i} ds \quad (15)$$

According to Equation (13), by defining $z = \psi(\omega, \varepsilon_0)s$, the i th order fractional derivative of stress with intrinsic time has the form

$$D^i[\sigma(u)] = \frac{d^i}{dt^i}\sigma(u) = \frac{1}{\Gamma(1-i)} \int_0^u \frac{\dot{\sigma}(z)}{(u-z)^i} dz = \frac{1}{\psi^i(\omega, \varepsilon_0)\Gamma(1-i)} \int_0^t \frac{\dot{\sigma}(s)}{(t-s)^i} ds \quad (16)$$

Then, we obtain

$$D^i[\sigma(u)] = \frac{1}{\psi^i(\omega, \varepsilon_0)} D^i[\sigma(t)] \quad (17)$$

It also can be obtained that

$$D^i[\varepsilon(u)] = \frac{1}{\psi^i(\omega, \varepsilon_0)} D^i[\varepsilon(t)] \quad (18)$$

By replacing the physical time t in the constitutive equation of viscoelastic materials in Equation (8) with the intrinsic time $u(t)$, the viscoelastic constitutive equation based on the internal variable theory can be obtained as

$$\begin{aligned} & \frac{c_2}{\eta_1}\sigma(t) + \frac{1}{\eta_1\psi^\alpha}D^\alpha\sigma(t) \\ &= \frac{1}{\psi^{\alpha+\gamma}}D^{\alpha+\gamma}\varepsilon(t) + \frac{c_1}{\psi^\alpha}D^\alpha\varepsilon(t) + \frac{\mu_2}{\eta_1\psi^\beta}D^\beta\varepsilon(t) + \frac{c_2}{\psi^\gamma}D^\gamma\varepsilon(t) + c_1c_2\varepsilon(t) \end{aligned} \quad (19)$$

Then, Equations (10) and (11) can be rewritten as

$$\begin{aligned} G_1 &= \mu_1 + \eta_1(\omega/\psi)^\gamma \cos(\gamma\pi/2) \\ &+ \frac{\mu_2c_2(\omega/\psi)^\beta \cos(\beta\pi/2) + \mu_2(\omega/\psi)^{\alpha+\beta} \cos[(\alpha-\beta)\pi/2]}{c_2^2 + 2c_2(\omega/\psi)^\alpha \cos(\alpha\pi/2) + (\omega/\psi)^{2\alpha}} \end{aligned} \quad (20)$$

$$\begin{aligned} G_2 &= \eta_1(\omega/\psi)^\gamma \sin(\gamma\pi/2) \\ &+ \frac{\mu_2c_2(\omega/\psi)^\beta \sin(\beta\pi/2) + \mu_2(\omega/\psi)^{\alpha+\beta} \sin[(\beta-\alpha)\pi/2]}{c_2^2 + 2c_2(\omega/\psi)^\alpha \cos(\alpha\pi/2) + (\omega/\psi)^{2\alpha}} \end{aligned} \quad (21)$$

The performance of viscoelastic dampers is significantly affected by ambient temperature and excitation frequency, and temperature and frequency impacts are closely related. Especially for the temperature regions of T_g to $T_g + 100$ °C, the storage modulus and loss modulus at high frequency are equal to those at low temperature, and the dynamic modulus at low frequency are also equivalent to those at high temperature, which has been defined as the temperature–frequency equivalent principle [38]:

$$\begin{aligned} G_1(\omega, T) &= G_1(a_T\omega, T_0) \\ \eta(\omega, T) &= \eta(a_T\omega, T_0) \end{aligned} \quad (22)$$

where T_g is the glass transition temperature, a_T is the shaft factor, and $a_T = 10^{-12(T-T_0)/[525+(T-T_0)]}$. T represents the environmental temperature and T_0 is the reference temperature. By applying Equation (22) to Equations (20) and (21), we have

$$\begin{aligned} G_1 &= \mu_1 + \eta_1(a_T\omega/\psi)^\gamma \cos(\gamma\pi/2) \\ &+ \frac{\mu_2c_2(a_T\omega/\psi)^\beta \cos(\beta\pi/2) + \mu_2(a_T\omega/\psi)^{\alpha+\beta} \cos[(\alpha-\beta)\pi/2]}{c_2^2 + 2c_2(a_T\omega/\psi)^\alpha \cos(\alpha\pi/2) + (a_T\omega/\psi)^{2\alpha}} \end{aligned} \quad (23)$$

$$G_2 = \eta_1(\alpha_T\omega/\psi)^\gamma \sin(\gamma\pi/2) + \frac{\mu_2 c_2 (\alpha_T\omega/\psi)^\beta \sin(\beta\pi/2) + \mu_2 (\alpha_T\omega/\psi)^{\alpha+\beta} \sin[(\beta - \alpha)\pi/2]}{c_2^2 + 2c_2(\alpha_T\omega/\psi)^\alpha \cos(\alpha\pi/2) + (\alpha_T\omega/\psi)^{2\alpha}} \quad (24)$$

Equations (22)–(24) are the expressions of the higher-order fractional derivative model modified with the internal variable theory and temperature–frequency equivalent principle (ITHF), which can reflect the impacts of surrounding temperature, excitation frequency, and loading displacement/strain amplitude on the dynamic behaviors of viscoelastic dampers well.

4. Experiments Verification

To verify the effectiveness and progressiveness of the ITHF model in describing the dynamic behaviors of viscoelastic dampers with changing displacement amplitudes and frequencies, the Kraus model [24] is introduced to modify the higher-order fractional derivative model and the comparisons of the experimental and numerical results of the viscoelastic damper are conducted. According to the Kraus model, the storage modulus $G_1(\varepsilon)$ is proportional to $\frac{1}{1+(\varepsilon/\varepsilon_c)^{2m}}$, and the loss modulus $G_2(\varepsilon)$ is proportional to $\frac{2(\varepsilon/\varepsilon_c)^m}{1+(\varepsilon/\varepsilon_c)^{2m}}$, as seen below.

$$\begin{cases} G_1(\varepsilon) = G_1(0) - \bar{G}_1 + \frac{\bar{G}_1}{1 + (\varepsilon/\varepsilon_c)^{2m}}; \\ G_2(\varepsilon) = G_2^\infty + \frac{2(G_2^{\max} - G_2^\infty)(\varepsilon/\varepsilon_c)^m}{1 + (\varepsilon/\varepsilon_c)^{2m}}. \end{cases} \quad (25)$$

where $G_1(0)$, \bar{G}_1 , G_2^∞ , G_2^{\max} , ε_c , and m are constants. By applying Equations (22) and (25) to Equations (10) and (11), the higher-order fractional derivative model modified with the Kraus model and temperature–frequency equivalent principle (KTHF) can be obtained as

$$G_1 = k_1 \left\{ \begin{array}{l} \mu_1 + \eta_1(\alpha_T\omega)^\gamma \cos(\gamma\pi/2) \\ + \frac{\mu_2 c_2 (\alpha_T\omega)^\beta \cos(\beta\pi/2) + \mu_2 (\alpha_T\omega)^{\alpha+\beta} \cos[(\alpha - \beta)\pi/2]}{c_2^2 + 2c_2(\alpha_T\omega)^\alpha \cos(\alpha\pi/2) + (\alpha_T\omega)^{2\alpha}} \end{array} \right\} \frac{1}{1 + (\varepsilon/\varepsilon_c)^{2m}} + b_1 \quad (26)$$

$$G_2 = k_2 \left\{ \begin{array}{l} \eta_1(\alpha_T\omega)^\gamma \sin(\gamma\pi/2) \\ + \frac{\mu_2 c_2 (\alpha_T\omega)^\beta \sin(\beta\pi/2) + \mu_2 (\alpha_T\omega)^{\alpha+\beta} \sin[(\beta - \alpha)\pi/2]}{c_2^2 + 2c_2(\alpha_T\omega)^\alpha \cos(\alpha\pi/2) + (\alpha_T\omega)^{2\alpha}} \end{array} \right\} \frac{2(\varepsilon/\varepsilon_c)^m}{1 + (\varepsilon/\varepsilon_c)^{2m}} + b_2 \quad (27)$$

where k_1 , b_1 , k_2 , and b_2 are material parameters.

The least squares method is utilized for parameter identification of the models. By optimizing $\min F(\omega, \varepsilon, T)$ in Equation (28) with test data of the storage modulus G_1 and the loss factor η , the parameters of the ITHF model and KTHF models can be achieved.

$$F(\omega, \varepsilon, T) = p_1 \{ [G_1(\omega, \varepsilon, T) - G_{10}(\omega, \varepsilon, T)] / G_{10}(\omega, \varepsilon, T) \}^2 + p_2 \{ [\eta(\omega, \varepsilon, T) - \eta_0(\omega, \varepsilon, T)] / \eta_0(\omega, \varepsilon, T) \}^2 \quad (28)$$

where p_1 and p_2 are weighting parameters, $p_1 + p_2 = 1.0$, $G_1(\omega, \varepsilon, T)$ and $\eta(\omega, \varepsilon, T)$ are numerical results, and $G_{10}(\omega, \varepsilon, T)$ and $\eta_0(\omega, \varepsilon, T)$ are experimental results.

Some experimental data from the viscoelastic damper with randomly selected frequencies and displacement amplitudes are used for data fitting, and the parameters of the ITHF model are determined as $\mu_1 = 3.695 \times 10^5$, $\eta_1 = 2.0993 \times 10^{-9}$, $\mu_2 = 6.3021 \times 10^5$, $c_2 = 1.2507 \times 10^3$, $\chi = 0.6368$, $\zeta = 0.7114$, $\alpha = 0.0853$, $\beta = 0.2187$, $\gamma = 0.9654$, and $T_0 = 570.2816$ K. Similarly, the parameters of the KTHF model are also determined as $\mu_1 = 1.6086 \times 10^{10}$, $\eta_1 = 3.8768 \times 10^8$, $\mu_2 = 7.0468 \times 10^8$, $c_2 = 3.4705 \times 10^8$, $\alpha = 0.1766$, $\beta = 0.5678$, $\gamma = 0.2032$, $k_1 = 2.2937 \times 10^{-8}$, $b_1 = 8.0575 \times 10^5$, $k_2 = 1.1537 \times 10^{-8}$, $b_2 = 5.2489 \times 10^4$, $\varepsilon_c = 0.0125$,

$m = 0.3685$, and $T_0 = 634.3185$ K. The comparisons of the numerical results of the ITHF model, KTHF model, and experimental results with frequency 1.0 Hz and displacement 1.0 mm are presented in Figure 8a,b, respectively.

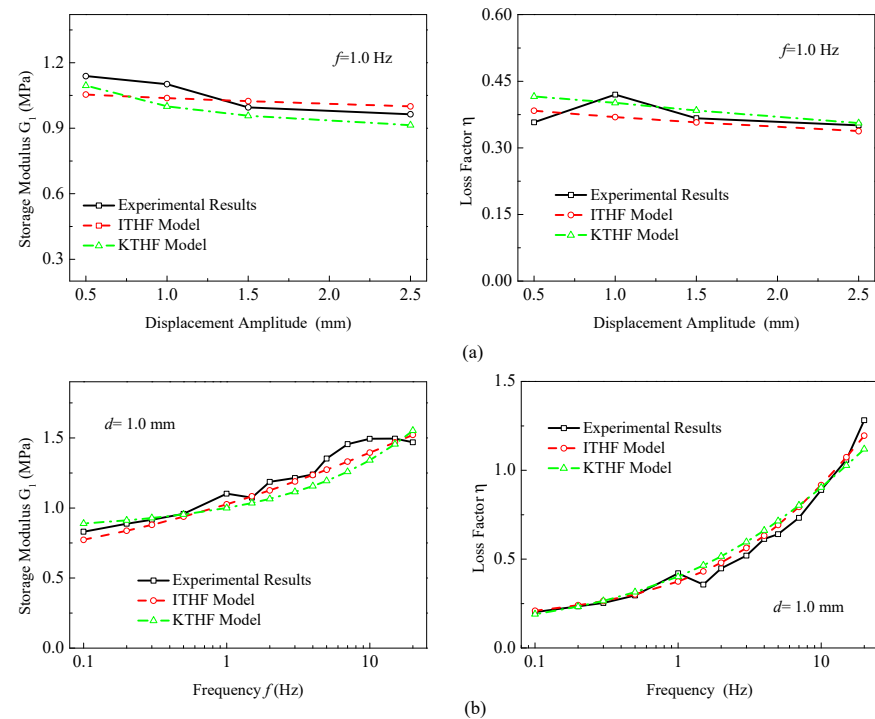


Figure 8. Comparisons of test data and numerical results for ITHF model and KTHF model. (a) $f = 1.0$ Hz. (b) $d = 1.0$ mm.

Figure 8a shows the experimental and numerical results of the storage modulus and loss factor with varying displacement amplitudes when $f = 1.0$ Hz. It reveals that the deviations of numerical results of both the ITHF model and the KTHF model from the experimental results are very small. The experimental and numerical results of the viscoelastic damper with changing displacement amplitudes are given in Table 6. For the storage modulus with frequency 1.0 Hz, the maximum error and root mean square error of the ITHF model in different displacement amplitudes are 7.44% and 5.28%, respectively, and the maximum error and root mean square error of the KTHF model in different displacement amplitudes are 8.59% and 6.03%, respectively. For the loss factor, the maximum error and root mean square error of the ITHF model with different displacement amplitudes are 12.04% and 7.38%, respectively, and the maximum error and root mean square error of the KTHF model in different displacement amplitudes are 16.25% and 8.78%, respectively. The ITHF model is more accurate in reflecting the dynamic behaviors of viscoelastic dampers with changing displacement amplitudes.

The experimental and numerical result comparisons with varying frequencies at displacement amplitude 1 mm are shown in Figure 8b, and the test and numerical data with the ITHF model and KTHF model are listed in Table 7. The maximum error and root mean square error of the ITHF model for the storage modulus in different frequencies are 8.53% and 4.98%, respectively, and the maximum error and root mean square error of the KTHF model for the storage modulus in different frequencies are 15.08% and 6.34%, respectively. The maximum error and root mean square error of the ITHF model for the loss factor in different frequencies are 20.98% and 8.13%, respectively, and the maximum error and root mean square error of the KTHF model for the loss factor in different frequencies are 30.34% and 11.79%, respectively.

Table 6. The comparisons of the ITHF model and KTHF model when $f = 1.0$ Hz.

Displacement Amplitude d (mm)	Characteristic Parameters	Experimental Results	Numerical Results			
			ITHF Model	Error	KTHF Model	Error
0.5	G_1 (MPa)	1.1385	1.0538	7.44%	1.0953	3.94%
	η	0.3576	0.3836	7.23%	0.4157	16.25%
1	G_1 (MPa)	1.1018	1.0379	5.8%	1	3.64%
	η	0.42	0.3694	12.04%	0.4015	4.41%
1.5	G_1 (MPa)	0.9952	1.0238	2.87%	0.96	6.54%
	η	0.3666	0.3573	2.53%	0.3841	4.78%
2.5	G_1 (MPa)	0.9638	1	3.76%	0.91	8.59%
	η	0.3506	0.3377	3.68%	0.3559	1.5%

Table 7. The comparisons of the ITHF model and KTHF model when $d = 1.0$ mm.

Frequency f (Hz)	Characteristic Parameters	Experimental Results	Numerical Results			
			ITHF Model	Error	KTHF Model	Error
0.1	G_1 (MPa)	0.8309	0.7729	6.98%	0.8895	15.08%
	η	0.2022	0.2093	3.51%	0.1902	5.96%
0.2	G_1 (MPa)	0.8874	0.8376	5.62%	0.9117	8.85%
	η	0.2342	0.2405	2.67%	0.233	0.51%
0.3	G_1 (MPa)	0.9158	0.8798	3.93%	0.9282	5.5%
	η	0.2533	0.2641	4.25%	0.2651	4.65%
0.5	G_1 (MPa)	0.9582	0.938	2.11%	0.9538	1.69%
	η	0.296	0.302	2.02%	0.3146	6.28%
1	G_1 (MPa)	1.1018	1.0263	6.85%	1	2.56%
	η	0.42	0.3741	10.93%	0.4015	4.41%
1.5	G_1 (MPa)	1.0734	1.0831	0.9%	1.0352	4.42%
	η	0.3565	0.4313	20.98%	0.4647	30.35%
2	G_1 (MPa)	1.1868	1.1256	5.15%	1.0648	5.4%
	η	0.4482	0.4803	7.15%	0.5157	15.06%
3	G_1 (MPa)	1.2141	1.1887	2.09%	1.1145	6.25%
	η	0.5197	0.5629	8.31%	0.597	14.86%
4	G_1 (MPa)	1.2393	1.2356	0.3%	1.1565	6.4%
	η	0.614	0.6322	2.97%	0.6614	7.72%
5	G_1 (MPa)	1.3529	1.273	5.91%	1.1935	6.24%
	η	0.6407	0.6925	8.08	0.7153	11.65%
7	G_1 (MPa)	1.4552	1.3311	8.53%	1.2582	5.47%
	η	0.7325	0.7944	8.45%	0.803	9.62%
10	G_1 (MPa)	1.4936	1.3945	6.64%	1.3404	3.87%
	η	0.8891	0.9171	3.14%	0.9038	1.66%
15	G_1 (MPa)	1.4949	1.4684	1.78%	1.4547	0.93%
	η	1.0592	1.0739	1.38%	1.0272	3.02%
20	G_1 (MPa)	1.4687	1.5217	3.61%	1.5521	2%
	η	1.2819	1.1954	6.75%	1.1194	12.67%

The ITHF model possesses enough precision in characterizing the dynamic and damping properties of the viscoelastic damper with changing displacement amplitudes and frequencies, and is more accurate than the KTHF model because it introduces the internal variable theory at the microscale to consider the displacement amplitude impacts. The

ITHF model has fewer parameters than the KTHF model and is more appropriate to be utilized in describing the dynamic properties of viscoelastic dampers.

5. Conclusions

Viscoelastic dampers are well-known passive vibration control devices and have been widely used in seismic/wind vibration control, micro vibration suppression, and platform vibration isolation, etc. In the present work, the dynamic properties of a viscoelastic damper at room temperature (18 °C) are tested under sinusoidal displacement excitations with a wide frequency band (0.1–25 Hz). The impacts of frequency and displacement amplitude on the dynamic properties of the viscoelastic damper are discussed. The higher-order fractional derivative model and the temperature–frequency equivalent principle are employed to characterize the frequency and temperature influence, and the internal variable theory considering the microscale structure influence is introduced to reflect the displacement amplitude affection. The ITHF model is proposed and verified with experimental results. Some notable conclusions can be obtained, such as:

- (1) The viscoelastic damper has great energy dissipation properties at room temperature with frequencies 0.1 Hz~25 Hz, especially at high frequencies (1 Hz~25 Hz). The damping performance and stiffness of the damper are crucially affected by the excitation frequency, while the damping performance is greatly influenced by the displacement amplitude, and the stiffness is slightly affected.
- (2) The characteristic parameters of viscoelastic dampers are significantly dependent on the external excitation frequencies and loading amplitudes. The parameters G_1 , G_2 , η , E_d , and K_e increase remarkably with increasing frequency, while C_e decreases. The energy dissipation E_d rises prominently with displacement amplitude, while and other parameters reduce mildly.
- (3) The ITHF model possesses enough precision in characterizing the dynamic and damping properties of viscoelastic dampers with changing displacement amplitudes and frequencies, and has higher accuracy and fewer parameters than the KTHF model.
- (4) The ITHF model introduces the internal variable theory to reflect the displacement amplitude impacts, which considers the internal structures' evolution process at the microscale and is of great significance for material design and damping property improvement.

Author Contributions: Conceptualization, Y.X.; data curation, X.-H.H. and Y.-Q.G.; formal analysis, Y.X., Q.H.; funding acquisition, Y.X. and Y.-Q.G.; investigation, Q.H. and X.-H.H.; methodology, Y.X., J.K.; resources, Y.X.; software, Y.-R.D. and Z.-W.H.; supervision, Y.-Q.G.; validation, Y.X., X.-H.H., Y.-R.D. and Q.H.; writing—original draft, Y.X.; writing—review and editing, Q.H. and Y.-Q.G. and J.K. All authors have read and agreed to the published version of the manuscript.

Funding: This study was financially supported by the National Natural Science Foundation of China with Grant No. 52108443, 52278505, the Jiangsu Province International Cooperation Project with Grant No. SBZ2022000169, National Key Research and Development Plans with Grant No. 2019YFE0121900, the Zhi Shan Scholarship of Southeast University with Grant No. 2242022R40041, the Innovation and Entrepreneurship Program (Innovation and entrepreneurship Doctor) of Jiangsu Province with Grant No. JSSCBS20210132, the Fundamental Research Funds for the Central Universities, the National Natural Science Foundation of China with Grant No. 52208503, and the Key Project of Collaborative Innovation Center of Shaanxi Provincial Department of Education with Grant No. 22JY029.

Informed Consent Statement: Not applicable.

Data Availability Statement: The data presented in this study are available on request from the corresponding author. The data are not publicly available due to the confidentiality requirements of the lab.

Acknowledgments: The authors are thankful for the help of Yonggang Huang's research group in Northwestern University (Evanston, IL 60201, U.S.).

Conflicts of Interest: The authors declare no conflict of interest. The funders had no role in the design of the study, in the collection, analyses, or interpretation of data, in the writing of the manuscript, or in the decision to publish the results.

Nomenclature

u_d	Displacement of the viscoelastic damper
u_0	Displacement amplitude of the damper
f	Loading frequency
ω	Angular frequency of the sinusoidal displacement loading.
d	Excitation displacement amplitude
F_d	Damping force of the viscoelastic damper at u_d
F_1	Damping force of the viscoelastic damper at u_0
K_e	Equivalent stiffness of the viscoelastic damper
F_2	Damping force when $u_d = 0$
F	Biggest damping force at each hysteresis curve
G_1	Storage modulus of the viscoelastic material/damper
G_2	Loss modulus of the viscoelastic material/damper
η	Loss factor of the viscoelastic material/damper
E_d	Energy dissipation of the viscoelastic damper at each hysteresis curve
K_e	Equivalent stiffness of the viscoelastic damper
C_e	Equivalent damping of the viscoelastic damper
h_v	Thickness of the viscoelastic layers of the viscoelastic damper
n_v	Number of viscoelastic layers of the viscoelastic damper
A_v	Shear area of viscoelastic layers of the viscoelastic damper
μ_1, μ_2	Elastic modulus of the spring elements
η_1, η_2	Viscous parameters of the fractional dashpots
D^i	i th order fractional derivative, $i = \alpha, \beta, \gamma$, etc.
t	Time
$u(t)$	Intrinsic time
ε_0	Excitation strain amplitude.
$\psi(\omega, \varepsilon_0)$	Reduction factor
χ, ζ	Material parameters considering the internal variable theory
T_g	Glass transition temperature
T	Temperature
T_0	Reference temperature
a_T	Shift factor
$G_1(0), \bar{G}_1, G_2^\infty, G_2^{\max}$	Storage modulus with initial strain, difference between the storage modulus of an arbitrary strain and that of an infinite strain, loss modulus of an infinite strain, and the maximum loss modulus
ε_c	Characteristic strain
m	Fractal dimension of filler structures
k_1, b_1, k_2, b_2	Linear regression parameters
$F(\omega, \varepsilon, T), p_1, p_2$	Objective optimization function and weighting parameters

References

- Xu, Z.D. Earthquake mitigation study on viscoelastic dampers for reinforced concrete structures. *J. Vib. Control.* **2007**, *13*, 29–45. [[CrossRef](#)]
- Mazza, F.; Vulcano, A. Control of the earthquake and wind dynamic response of steel-framed buildings by using additional braces and/or viscoelastic dampers. *Earthq. Eng. Struct. Dyn.* **2011**, *40*, 155–174. [[CrossRef](#)]
- Lee, D.O.; Park, G.; Han, J.H. Hybrid isolation of micro vibrations induced by reaction wheels. *J. Sound Vib.* **2015**, *363*, 1–17. [[CrossRef](#)]
- Xu, Z.D.; Huang, X.H.; Xu, F.H.; Yuan, J. Parameters optimization of vibration isolation and mitigation system for precision platforms using non-dominated sorting genetic algorithm. *Mech. Syst. Signal Process.* **2019**, *128*, 191–201. [[CrossRef](#)]
- Xu, Z.D.; Xu, C.; Hu, J. Equivalent fractional Kelvin model and experimental study on viscoelastic damper. *J. Vib. Control.* **2015**, *21*, 2536–2552. [[CrossRef](#)]
- Dai, J.; Xu, Z.D.; Gai, P.P.; Hu, Z.W. Optimal design of tuned mass damper inerter with a Maxwell element for mitigating the vortex-induced vibration in bridges. *Mech. Syst. Signal.* **2021**, *148*, 107180. [[CrossRef](#)]

7. Zhou, X.Q.; Yu, D.Y.; Shao, X.Y.; Zhang, S.Q.; Wang, S. Research and applications of viscoelastic vibration damping materials: A review. *Compos. Struct.* **2016**, *136*, 460–480. [CrossRef]
8. Wang, S.J.; Chiu, I.C.; Yu, C.H.; Zhang, Q.Y.; Chang, K.C. Experimental beyond design and residual performances of full-scale viscoelastic dampers and their empirical modeling. *Earthq. Engng. Struct. Dyn.* **2019**, *48*, 1093–1111. [CrossRef]
9. Ge, T.; Xu, Z.D.; Yuan, F.G. Development of viscoelastic damper based on NBR and organic small-molecule composites. *J. Mater. Civil Eng. ASCE* **2022**, *34*, 04022192. [CrossRef]
10. Zhang, R.H.; Soong, T.T. Seismic design of viscoelastic dampers for structural applications. *J. Struct. Eng.* **1992**, *118*, 1375–1392. [CrossRef]
11. Aprile, A.; Jose, A.I.; James, M.K. Evolutionary model of viscoelastic dampers for structural applications. *J. Eng. Mech. ASCE* **1997**, *123*, 551–560. [CrossRef]
12. Tsai, C.S. Temperature effect of viscoelastic dampers during earthquakes. *J. Struct. Eng. ASCE* **1994**, *120*, 394–409. [CrossRef]
13. Cazenove, J.; Rade, D.A.; Lima, A.M.G.D.; Araújo, C.A. A numerical and experimental investigation on self-heating effects in viscoelastic dampers. *Mech. Syst. Signal Process.* **2012**, *27*, 433–445. [CrossRef]
14. Xu, Z.D.; Liao, Y.X.; Ge, T.; Xu, C. Experimental and theoretical study on viscoelastic dampers with different matrix rubbers. *J. Eng. Mech. ASCE* **2016**, *142*, 04016051. [CrossRef]
15. Xu, Z.D.; Shen, Y.P.; Zhao, H.T. A synthetic optimization analysis method on structures with viscoelastic dampers. *Soil Dyn. Earthq. Eng.* **2003**, *23*, 683–689. [CrossRef]
16. Xu, Z.D.; Zhao, H.T.; Li, A.Q. Optimal analysis and experimental study on structures with viscoelastic dampers. *J. Sound Vib.* **2004**, *273*, 607–618. [CrossRef]
17. Xu, Z.D. Horizontal shaking table tests on structures using innovative earthquake mitigation devices. *J. Sound Vib.* **2009**, *325*, 34–48. [CrossRef]
18. Xu, Z.D.; Huang, X.H.; Lu, L.H. Experimental study on horizontal performance of multi-dimensional earthquake isolation and mitigation devices for long-span reticulated structures. *J. Vib. Control.* **2012**, *18*, 941–952. [CrossRef]
19. Sato, D.; Osabel, D.M.; Kasai, K. Evaluation method for practical application of viscoelastic damper using equivalent sinusoidal waveforms of long-duration random excitations in along- and across-wind directions. *Eng. Struct.* **2022**, *254*, 113735. [CrossRef]
20. Xu, C.; Xu, Z.D.; Huang, X.H.; Xu, Y.S.; Ge, T. Modeling and analysis of a viscoelastic micro-vibration isolation and mitigation platform for spacecraft. *J. Vib. Control.* **2018**, *24*, 4337–4352. [CrossRef]
21. He, X.Y.; Zhao, T.W.; Li, H.N.; Zhang, J. Multi-dimensional seismic response control of offshore platform structures with viscoelastic dampers (II-Experimental study). *Struct. Monit. Maint.* **2016**, *3*, 175–194. [CrossRef]
22. Lakes, R. *Viscoelastic Materials*; Cambridge University Press: New York, NY, USA, 2009. [CrossRef]
23. Tsai, C.S.; Lee, H.H. Applications of viscoelastic dampers to high-rise buildings. *J. Struct. Eng. ASCE* **1993**, *120*, 1222–1233. [CrossRef]
24. Payne, A.R. The dynamic properties of carbon black-loaded natural rubber vulcanizates. Part I. *J. Appl. Polym. Sci.* **1962**, *6*, 57–63. [CrossRef]
25. Liang, Z.; Li, J.; Zhang, X.; Kan, Q. A viscoelastic-viscoplastic constitutive model and its finite element implementation of amorphous polymers. *Polym. Test.* **2023**, *117*, 107831. [CrossRef]
26. Bagley, R.L.; Torvik, P.J. Fractional calculus in the transient analysis of viscoelastically damped structures. *AIAA J.* **1985**, *23*, 918–925. [CrossRef]
27. Lewandowski, R. Influence of temperature on the dynamic characteristics of structures with viscoelastic dampers. *J. Struct. Eng. ASCE* **2018**, *145*, 04018245. [CrossRef]
28. Xu, Z.D.; Wang, D.X.; Shi, C.F. Model, tests and application design for viscoelastic dampers. *J. Vib. Control.* **2011**, *17*, 1359–1370. [CrossRef]
29. Xu, Z.D.; Ge, T.; Liu, J. Experimental and theoretical study of high-energy dissipation-viscoelastic dampers based on acrylate-rubber matrix. *J. Eng. Mech. ASCE* **2020**, *146*, 04020057. [CrossRef]
30. Conti, M.; Danese, V.; Pata, V. Aging of viscoelastic materials: A mathematical model. In *Mathematical Modeling in Cultural Heritage*; Springer: Cham, Switzerland, 2021; pp. 135–146. [CrossRef]
31. Wang, Q.; Gossweiler, G.R.; Craig, S.L.; Zhao, X.H. Mechanics of mechanochemically responsive elastomers. *J. Mech. Phys. Solids* **2015**, *82*, 320–344. [CrossRef]
32. Lu, D.; Xue, B.; Cao, Y.; Chen, B. Constitutive theory for direct coupling of molecular frictions and the viscoelasticity of soft materials. *J. Appl. Mech. ASME* **2022**, *89*, 051007. [CrossRef]
33. Biot, M.A. Theory of stress-strain relations in anisotropic viscoelasticity and relaxation phenomena. *J. Appl. Phys.* **1954**, *25*, 1385–1391. [CrossRef]
34. Eringen, A.C.; Paslay, P.R. Mechanics of continua. *Crop Pasture Sci.* **1968**, *52*, 397–413. [CrossRef]
35. Chang, K.C.; Lai, M.L.; Soong, T.T.; Hao, D.S.; Yeh, Y.C. *Seismic Behavior and Design Guidelines for Steel Frame Structures with Added Viscoelastic Dampers*, Technical Report NCEER-93-0009; Department of Civil Engineering, State University of New York: Buffalo, NY, USA, 1993; Available online: <https://hdl.handle.net/10477/748> (accessed on 10 October 2020).
36. Xu, Y.S.; Xu, Z.D.; Guo, Y.Q.; Ge, T.; Xu, C.; Huang, X.H. Theoretical and experimental study of viscoelastic damper based on fractional derivative approach and micromolecular structures. *J. Vib. Acoust. ASME* **2019**, *141*, 031010. [CrossRef]

37. Lion, A.; Kardelky, C. The Payne effect in finite viscoelasticity: Constitutive modelling based on fractional derivatives and intrinsic time scales. *Int. J. Plast.* **2004**, *20*, 1313–1345. [[CrossRef](#)]
38. Xu, Y.S.; Xu, Z.D.; Guo, Y.Q.; Jia, H.B.; Huang, X.H.; Wen, Y.W. Mathematical modeling and test verification of viscoelastic materials considering microstructures and ambient temperature influence. *Mech. Adv. Mater. Struct.* **2022**, *29*, 7063–7074. [[CrossRef](#)]

Disclaimer/Publisher’s Note: The statements, opinions and data contained in all publications are solely those of the individual author(s) and contributor(s) and not of MDPI and/or the editor(s). MDPI and/or the editor(s) disclaim responsibility for any injury to people or property resulting from any ideas, methods, instructions or products referred to in the content.